

## Accepted Manuscript

Sphere on Tile Ballistic Impact Experiment to Characterize the Response of Soda Lime Glass

Prusodman Sathananthan , Alexandra Sirois , Dilaver Singh , Duane Cronin

PII: S0734-743X(19)30456-7  
DOI: <https://doi.org/10.1016/j.ijimpeng.2019.103321>  
Article Number: 103321  
Reference: IE 103321



To appear in: *International Journal of Impact Engineering*

Received date: 3 May 2019  
Revised date: 13 June 2019  
Accepted date: 14 June 2019

Please cite this article as: Prusodman Sathananthan , Alexandra Sirois , Dilaver Singh , Duane Cronin , Sphere on Tile Ballistic Impact Experiment to Characterize the Response of Soda Lime Glass, *International Journal of Impact Engineering* (2019), doi: <https://doi.org/10.1016/j.ijimpeng.2019.103321>

This is a PDF file of an unedited manuscript that has been accepted for publication. As a service to our customers we are providing this early version of the manuscript. The manuscript will undergo copyediting, typesetting, and review of the resulting proof before it is published in its final form. Please note that during the production process errors may be discovered which could affect the content, and all legal disclaimers that apply to the journal pertain.

The final publication is available at Elsevier via <https://doi.org/10.1016/j.ijimpeng.2019.103321>. © 2019. This manuscript version is made available under the CC-BY-NC-ND 4.0 license <http://creativecommons.org/licenses/by-nc-nd/4.0/>

## Highlights

- Unconfined glass tiles were impacted with steel spheres at 100 to 800 m/s.
- Projectile velocities and damage progression within the tiles were repeatable.
- Impact features were quantified (fracture cones, cracking, and comminution).
- Tiles showed differing failure modes between non-perforating and perforating tests.
- Damage front speed varied; non-perforating (1500 m/s), perforating (3270 m/s).

ACCEPTED MANUSCRIPT

*An original article*

**Sphere on Tile Ballistic Impact Experiment to Characterize the Response of Soda Lime Glass**

Prusodman Sathananthan<sup>1</sup>, Alexandra Sirois<sup>2</sup>, Dilaver Singh<sup>1</sup>, Duane Cronin<sup>1</sup>

<sup>1</sup> University of Waterloo, Waterloo, ON, Canada

<sup>2</sup>DRDC Valcartier Research Center, Québec, Canada G3J 1X5

Submitted to International Journal of Impact Engineering

TBD

Corresponding Author: Duane Cronin, Ph.D.  
University of Waterloo  
200 University Avenue West  
Waterloo, ON, N2L 3G1, Canada  
Email: [duane.cronin@uwaterloo.ca](mailto:duane.cronin@uwaterloo.ca)  
Phone: 519-888-4567 x32682  
Fax: 519-885-5862

**Word Count:** Abstract: 234  
Introduction to Conclusions: (excluding captions, tables, etc.): 2584

**Keywords:** ballistic impact on ceramic, soda-lime silicate glass, sphere on glass tile

## Abstract

Robust computational models of soda-lime silicate glass (SLG) are used in the development of transparent armor systems, which require an independent set of experimental data with known boundary conditions for model validation. Although many experimental tests are presented in the literature, many of these tests incorporate complex boundary conditions or studied the impact of non-planar targets. A novel sphere on glass tile ballistic experiment was performed to quantify the damage features of planar impact, where an unconfined tile was impacted by a hardened steel sphere at velocities ranging from 100 m/s to 800 m/s. The impacts and resulting damage were recorded using high speed cameras.

Projectile kinematics and damage front propagation were successfully quantified and shown to be repeatable. A broad range of material damage was captured, including discrete fracture features such as fracture cones, radial cracks, concentric cracks, and material comminution. Three distinct impact responses were identified; non-perforating (100 - 500 m/s), transition (500 - 550 m/s) and perforating (550 - 800 m/s) that showed a transition in failure mode from discrete fracture (damage front  $\sim 1500$  m/s) to comminution (damage front, 3270 m/s) of the tile upon impact. The sphere on glass tile tests provided a repeatable set of experimental data to enable future comparison of the ballistic response of transparent materials, while providing simple boundary conditions that can be used to validate computational models of SLG over a range of impact velocities.

## 1. Introduction

Armored land vehicles rely on transparent armor to provide situational awareness and ballistic protection (Talladay et al., 2014). Transparent armor laminates, commonly incorporating soda-lime glass (SLG) owing to its low weight and excellent optical properties, experience a wide range of impacts, from rock strikes to small arms fire at a wide range of velocities. To aid in the development and optimization of transparent armor, computational models are often used to simulate impact scenarios, which requires experimental data to assess the fidelity of model predictions.

Ballistic impact of a projectile on ceramic materials is often described in three distinct phases: initial contact, localized damage, and finally structural response occurring later in time (Curran et al., 1994). When a projectile makes contact with a ceramic target, a shock wave forms at the impact location and propagates radially outward from the point of impact. Initially, the stresses are compressive and can reach magnitudes in the gigapascals (Chaudri, 2015). There are many types of waves that propagate through the material, at differing speeds, depending on the mechanical properties of the material (Meyers, 1994), and can result in different modes of damage and failure. When a compressive stress wave reaches the free surfaces of the target, the wave reflects in the opposite sense, resulting in a tensile release wave (Wilkins, 1978) and potentially spall of the ceramic material. Damage features can be broadly characterized into two groups; discrete fracture and comminution (Shockey et al., 1990). In discrete fracture, discrete cracks in soda lime silicate glass have been reported to travel at 1500 m/s (Küppers 1966, Barstow & Edgerton 1939, Nielsen 2009) and are associated with tensile stresses. The sustained

compressive stresses at the contact interface result in bulk failure of the material, which becomes pulverized, or comminuted. Comminution describes the coalescence of micro-fractures associated with compressive stresses. During edge-on impact experiments, comminution of glass was observed to be produced upon passage of a damage front which travelled at velocities of 3270 m/s (Grujicic, 2009), which is on the order of the shear wave speed in glass (3440 m/s, Dannemann 2011). A third common damage feature results from high tensile stresses at the surface of the target, which form shallow ring cracks that extend into the material at an angle ranging from 25° to 75° (Chaudri et al., 1978), coalescing into a fracture cone. For ballistic impacts on ceramic, the damage at the impact location can be described in terms four zones (Curran et al., 1994) (Figure 1). Closest to the point of impact is the Mescall zone (Zone 1), where material is finely comminuted. The Mescall zone is surrounded by a region of coarsely pulverized material (Zone 2). Outside the coarsely comminuted region is a zone of fractured material (Zone 3). And far enough from the point of impact, there is a region of largely intact material (Zone 4).

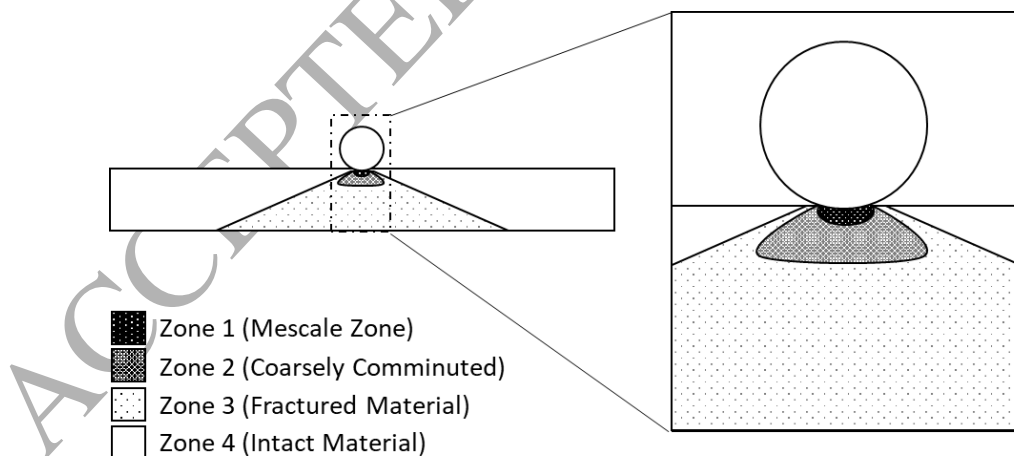


Figure 1: Zones of damage as described by Curran et al. (Curran et al., 1994).

Planar targets (e.g. tiles or transparent armor layers), typically have lengths and widths significantly larger than the depth or thickness. Consequently, planar targets typically experience high flexural stresses over their upper and lower surfaces, where bending stresses are at a maximum, and these stresses can result in the formation of concentric cracks (Thorton et al., 1986). The bending stresses can also generate radial cracks that extend outwards from the point of impact to the extremities of the target. If the target is sufficiently damaged, the projectile will pass through the target, resulting in perforation.

There are several studies in the literature focusing on impact tests on planar ceramic targets (Strassburger 2009, Anderson 2014, Hazell 2010, Compton et al. 2013); however, these tests are often performed on multi-layer laminates or on confined ceramics, making assessment of material model parameters difficult due to complex boundary conditions. Experimental tests that focus on damage characterization often use geometries that do not present major features of impact on planar ceramic targets. Such configurations include edge-on impacts (Strassburger, 2008), ceramic Taylor rod impacts (Willmot 2005), rod end impacts (Haney et al., 2012), and confined split Hopkinson bar experiments (Dannemann et al. 2011, Zhang et al. 2015). These tests allow for the visualization of damage propagation with respect to time, but do not allow for the tracking of features such as fracture cones, radial cracks and concentric cracks which are characteristics of impacts on planar targets (Cook & Pharr 1990, Thorton et al. 1986).

This study presents a novel set of impact experiments using a sphere on mono-material planar tile with simple boundary conditions, considering both perforating and non-perforating scenarios, and assessed using imaging diagnostics to quantify the nature and progression of damage.

## 2. Methods

The impact tests were undertaken on flat SLG tiles using spherical projectiles across a range of velocities from 100 m/s to 800 m/s. Hardened steel ball bearings (projectiles), 6.35 mm ( $\frac{1}{4}$ " in diameter) were contained in a sabot and accelerated using a fixed barrel, universal receiver setup (Figure 2). The targets were square, untreated, soda-lime glass tiles (Starphire, PPG Industries, Inc., Pittsburgh PA, Table 1) with dimensions of 101.6 x 101.6 x 12 mm ( $30.24 \text{ kg/m}^2$  areal density). A thickness of 12 mm was used because it was on the same order of magnitude as the diameter of many projectiles of interest, and similar to the thickness of a single layer of glass that may be used in fielded armor systems (Weinhold, 2013). The tiles were placed on a test bench perpendicular to the projectile path, and a small amount of ballistic clay was applied to position the tile and ensure the tiles were level while not interfering with the response of the tile. Three test repeats were performed at each impact velocity: 100 m/s, 200 m/s, 300 m/s, 500 m/s, 550 m/s, 650 m/s, and 800 m/s.

Table 1: Properties of soda-lime glass  
(Wereszczak and Anderson, 2014)

Property	Value
Density [ $\text{g/cm}^3$ ]	2.49
Elastic Modulus [GPa]	73.1
Poisson's Ratio [-]	0.203
Fracture Toughness [ $\text{MPa} \sqrt{\text{m}}$ ]	1.06



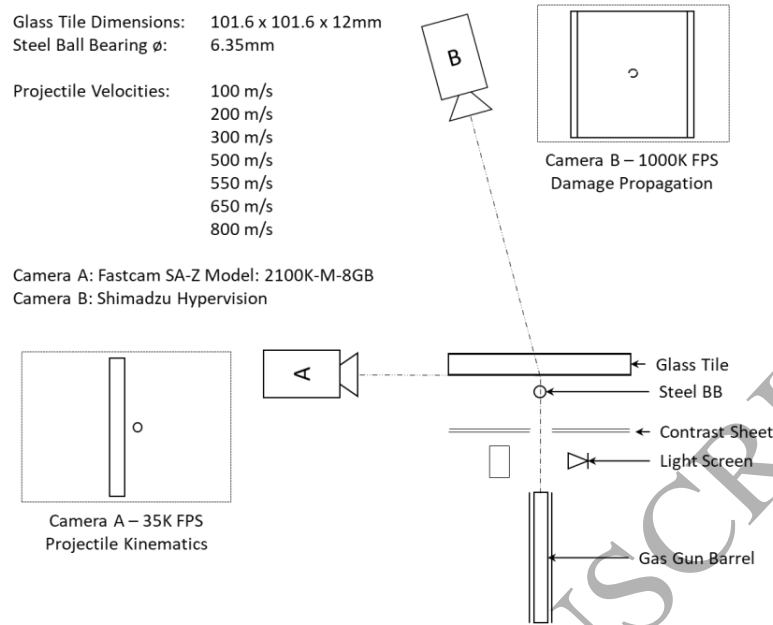


Figure 2: A schematic view of the experimental setup.

The impacts were recorded by two high speed cameras that were triggered by a light screen. The primary camera (Camera A, Fastcam SA-Z Model 2100K-M-8GB, IMAGICA Robot Holdings, Inc. (Photron), Tokyo, Japan) was set to a frame rate of 35 000 frames per second with a resolution of 1024x576 pixels to track the projectile. Camera A was placed orthogonal to the line of impact (Figure 2). The second camera (Camera B, Hypervision, Shimadzu Corp, Kyoto, Japan) was used to record damage propagation in the glass from a rear view of the target. Camera B was placed behind the target with respect to the point of impact and at a slight angle to allow for better visibility (the bullet trap was placed directly behind the target) and to prevent damage to the camera. Camera B was set to record with a frame rate of 1 000 000 frames per second and an effective resolution of 240 x 240 pixels (cropped from 400 x 250). Kinematic data, including projectile velocities and damage propagation velocities were obtained using a video analysis tool (Tracker, Open Source Physics).

## 2.1 Projectile Kinematics

To determine the projectile velocity, a single point on the sphere was tracked (Camera A, Figure 3). The diameter of the sphere and thickness of the tile were used for length calibration. This calibration was further verified by comparing the tracked projectile velocities with measured velocities from the light screens, all of which were in good agreement.

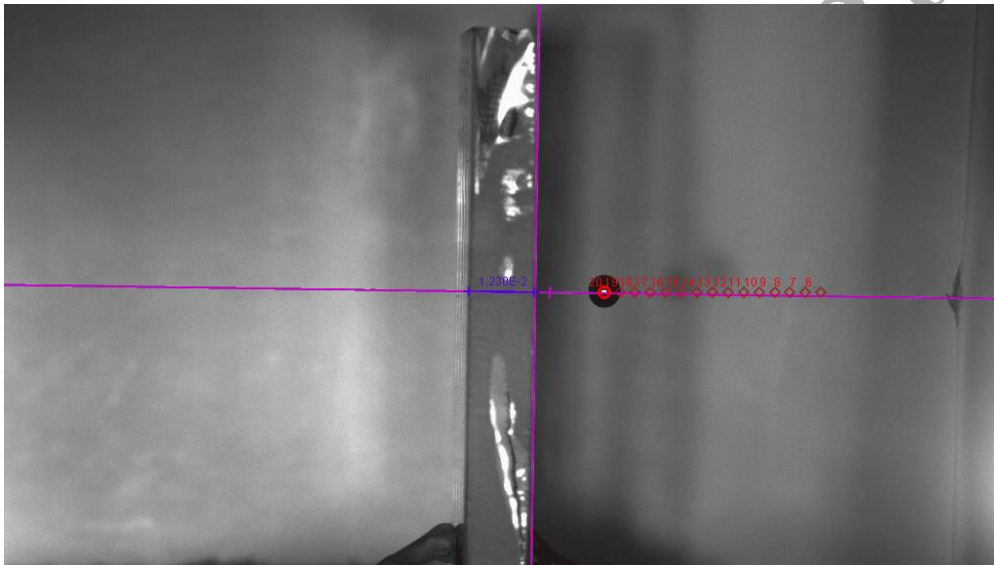


Figure 3: Tracking the position of the projectile over time using Tracker (100 m/s impact, Camera A).

The derivative of the displacement versus time data was taken to determine the projectile velocity. The initial and residual velocities were determined by finding the average velocity before and after the impact had occurred (Figure 4). In this study, all initial (or impact) velocities were taken as positive. If the projectile rebounded from the target surface, the residual velocity was taken as negative. If perforation occurred, the resulting velocity was taken as positive. For example, in the exemplar case, the initial velocity of the projectile was 100 m/s and the residual velocity was -31 m/s (the projectile rebounded at 31 m/s).

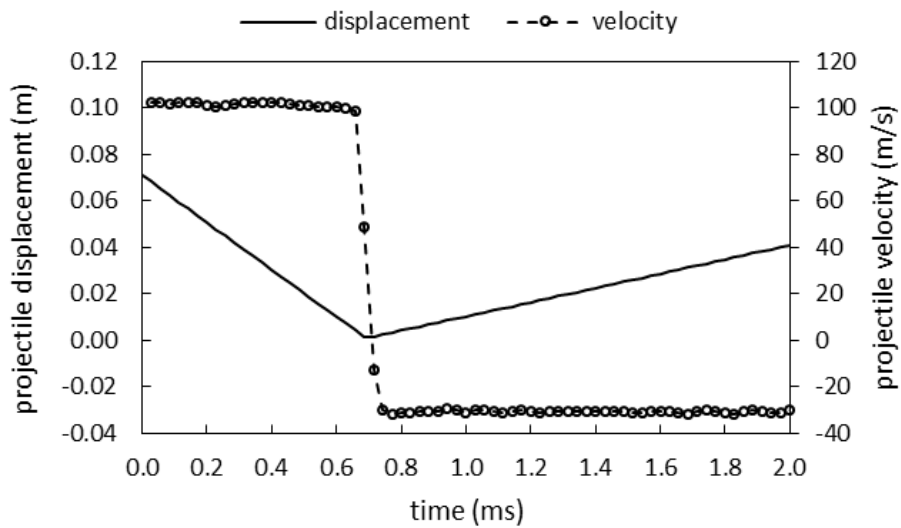


Figure 4: Exemplar displacement-time data used to determine initial and final velocities (100 m/s impact).

## 2.2 Features of Impact

Six features of impact were consistently observed in the tests, categorized as: discrete fracture (fracture cone, radial cracks, concentric cracks, edge cracks); material comminution; and perforation of the tile. Camera B was used to track damage in the tile over time including discrete cracks and comminution. The damage features were measured at 250  $\mu\text{s}$  after impact, well after the damage front had stopped progressing (50  $\mu\text{s}$  after impact). This study did not consider the damage accumulated during gross motion of the tile, which took place later in time.

## 2.3 Damage Front Tracking

Damage propagation was tracked using video from Camera B (Figure 5). To facilitate proper visualization of damage in the tile, a contrast sheet (white paper) was placed between the gas gun and the target. A rectangular window was cut in the contrast sheet to allow the projectile to pass

without tearing the sheet and obscuring the view (Figure 5). For the purposes of this study, the damage front was defined as the edge of damaged material (the boundary between visibly damaged and undamaged material, Figure 5), which originated from the point of impact. Radial and concentric cracks were excluded when measuring the damage front. The damage front was tracked in the one direction (vertical) since this provided the best contrast. The damage front was confirmed to be approximately circular by tracking damage at  $45^{\circ}$  intervals for a representative case (100 m/s), with a variation of 3-7% of the radius (standard deviation in the radius varying from 1.6 mm - 3.4mm over the impact event). Thus, it was deemed acceptable to measure the damage front in the vertical direction for the rest of the experiments.

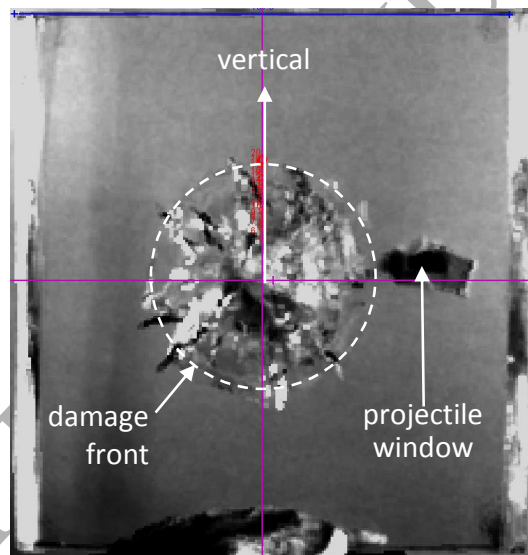


Figure 5: Tracking the position (red circles) of the damage front over time (100 m/s impact, Camera B).

### 3. Results

#### 3.1 Projectile Velocity

The initial and residual projectile velocities of the sphere on tile tests demonstrated good repeatability (Table 2). The tests captured both perforating and non-perforating events (Figure 6).

Table 2: Initial and residual projectile velocities.

$\pm$  = 1 standard deviation (coefficient of variation in brackets where applicable)

Experimental Data		Aggregate Results		
Initial Velocity (m/s)	Residual Velocity** (m/s)	Test Velocity (m/s)	Initial Velocity (m/s)	Residual Velocity (m/s)
103	-31	100	103 $\pm$ *	-31
-*	-*			
-*	-*			
200	-22	200	199 $\pm$ 1 (0.01)	-20 $\pm$ 2 (0.10)
199	-18			
198	-21			
299	-31			
300	-30			
302	-20	300	300 $\pm$ 2 (0.01)	-27 $\pm$ 6 (0.22)
497	-15			
504	-7	500	501 $\pm$ 4 (0.01)	-10 $\pm$ 5 (0.50)
503	-8			
567	-*			
565	-4	550	552 $\pm$ 24 (0.05)	2 $\pm$ 8 (4.00)
523	7			
648	60	650	652 $\pm$ 6 (0.01)	62 $\pm$ 3 (0.05)
649	60			
658	66			
805	129	800	805 $\pm$ *	129
-*	-*			
-*	-*			

\* Projectile not visible in high speed video before or after impact

\*\* Positive residual velocity indicates perforation

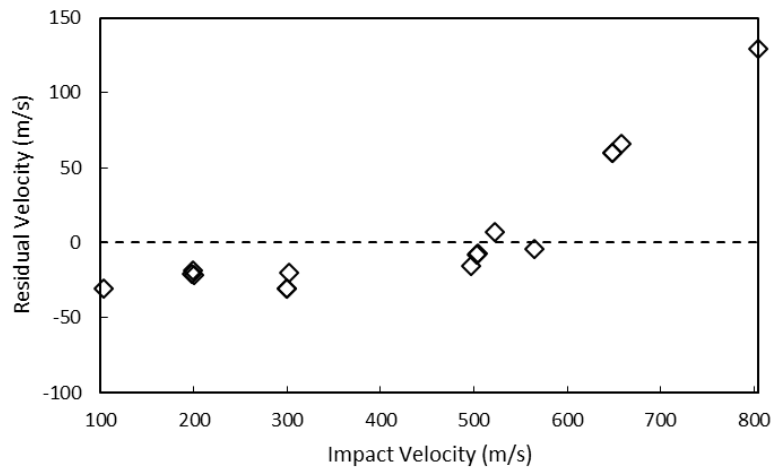


Figure 6: Residual velocity of projectiles versus impact velocity (+ = perforation, - = rebound).

### 3.2 Features of Impact

A variety of planar impact features were observed in the sphere on glass tile tests (Table 3) demonstrating a transition from discrete cracks to widespread comminution with increasing impact velocity. Interestingly, edge cracks were only identified at velocities in the transition from non-perforation to perforation. Many damage features such as the number of radial cracks and the radii of damage were consistent within test runs (Table 4). At a specific velocity, the damage progression was consistent between the three test repeats throughout the perforation process, demonstrating the repeatability of the test methodology (Appendix A). Not all planar impact features were present at every impact velocity. Different features of planar impact dominated at low (100 m/s), medium (500 m/s) and high (800 m/s) speed impacts (Figure 7). Damage progression analysis of other velocities can be found in Appendix B.

Table 3: Features of planar impact summary

Nominal Test Velocity	100 m/s	200 m/s	300 m/s	500 m/s	550 m/s	650 m/s	800 m/s
Fracture Cone	Yes	Yes	No	No	No	No	No
Radial Cracks	Yes	Yes	Yes	Partial	No	No	No
Concentric Cracks	No	Partial	Yes	Yes	No	No	No
Comminution	Yes	Yes	Yes	Yes	Yes	Yes	Yes
Edge Cracks	No	No	Yes	Yes	No	No	No
Perforation	No	No	No	No	Yes	Yes	Yes

Table 4: Number of radial cracks developed in target and damage front.  
 $\pm = 1$  standard deviation (coefficient of variation in brackets where applicable)

Experimental Data			Aggregate Results		
Impact Velocity (m/s)	Radial Cracks (#)	Damage Radius (Zone 3) (mm)	Nominal Test Velocity (m/s)	Radial Cracks (#)	Damage Radius (Zone 3) (mm)
103	8	26.9	100	8 $\pm$ 2 (0.25)	26 $\pm$ 3 (0.12)
-	6	28.2			
-	10	21.9			
200	17	21.8	200	16 $\pm$ 1 (0.06)	21 $\pm$ 4 (0.19)
199	16	21.5			
198	15	18.8			
299	31	33.5			
300	29	29.4	300	31 $\pm$ 3 (0.10)	31 $\pm$ 2 (0.06)
302	34	29.5			
497	-*	Whole Tile			
504	-*	Whole Tile	500	60	Whole Tile
503	60	Whole Tile			
567	-*	Whole Tile			
565	-*	Whole Tile	550	*	Whole Tile
523	-*	Whole Tile			
648	-*	Whole Tile			
649	-*	Whole Tile	650	*	Whole Tile
658	-*	Whole Tile			
805	-*	Whole Tile			
-	-*	Whole Tile	800	*	Whole Tile
-	-*	Whole Tile			

\* radial cracks not visible through comminution

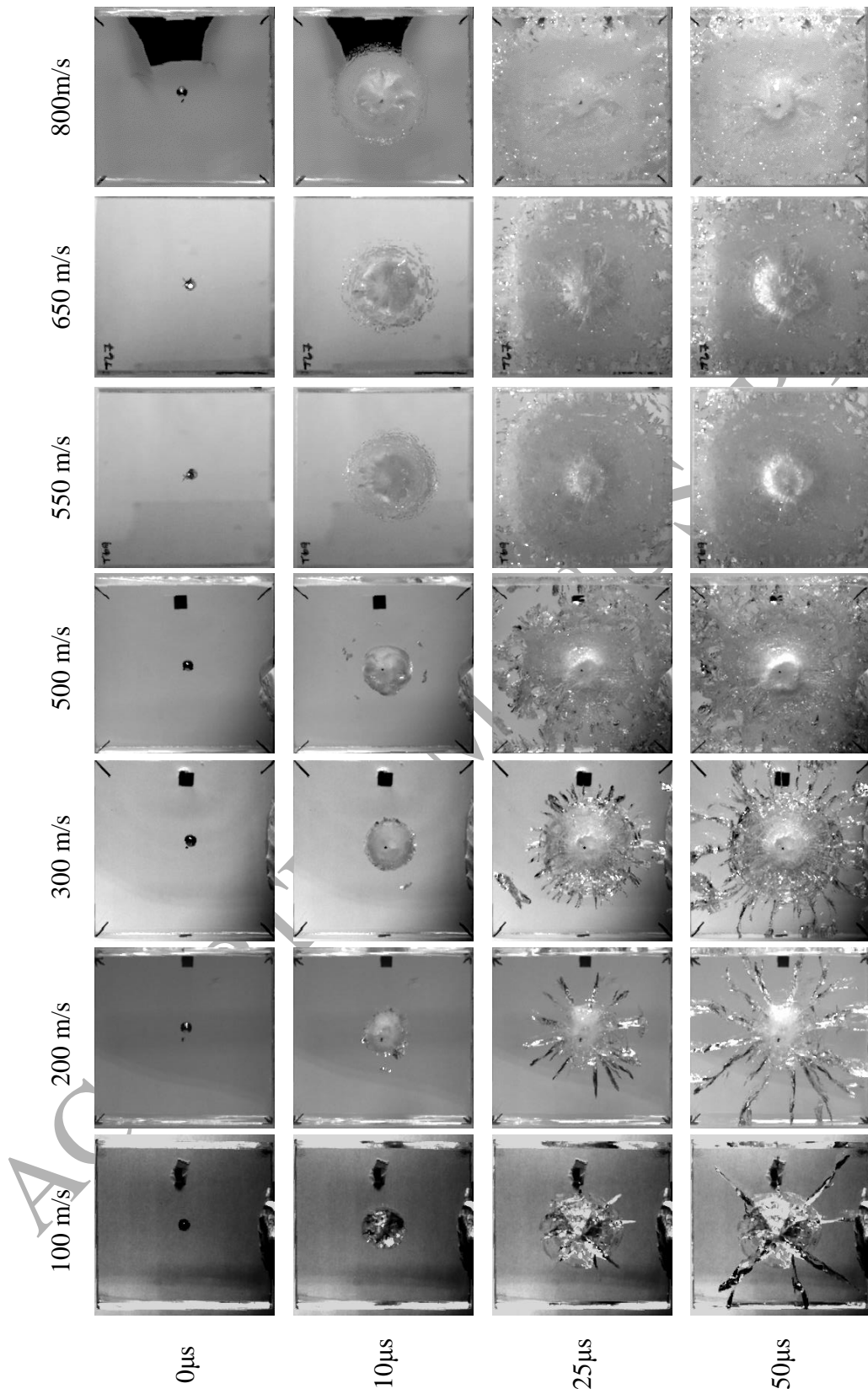


Figure 7: Damage propagation of representative tests at each velocity up to 50  $\mu$ s post-impact.



At low velocities (e.g. 100 m/s), discrete fracture was the primary mode of failure (Figure 8). A fracture cone formed over 25  $\mu$ s post impact (Figure 8A-C), and radial cracks extended to the edges of the tile (Figure 8D).

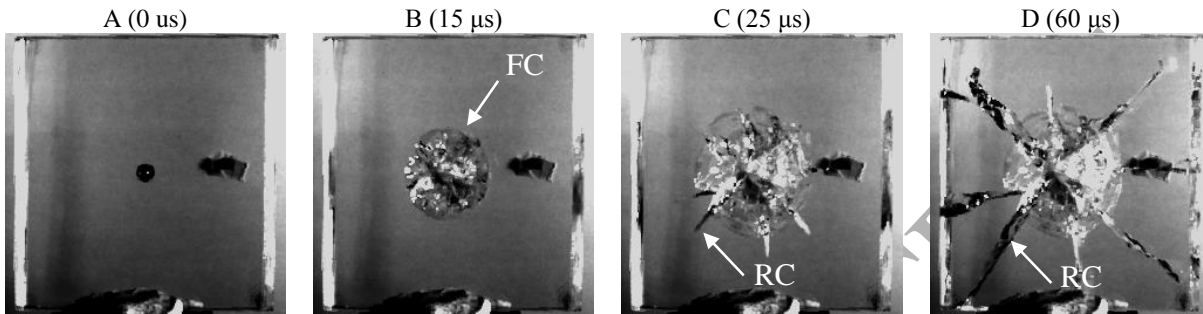


Figure 8: Progression of damage for a 100 m/s impact (FC = fracture cone, RC = radial crack).

At intermediate velocities (e.g. 500 m/s), comminution and discrete fracture were present (Figure 9). Discrete fracture preceded the damage front (Figure 9A), which in turn initiated further damage (Figure 9B), and eventually coalesced with the main damage front (Figure 9C).

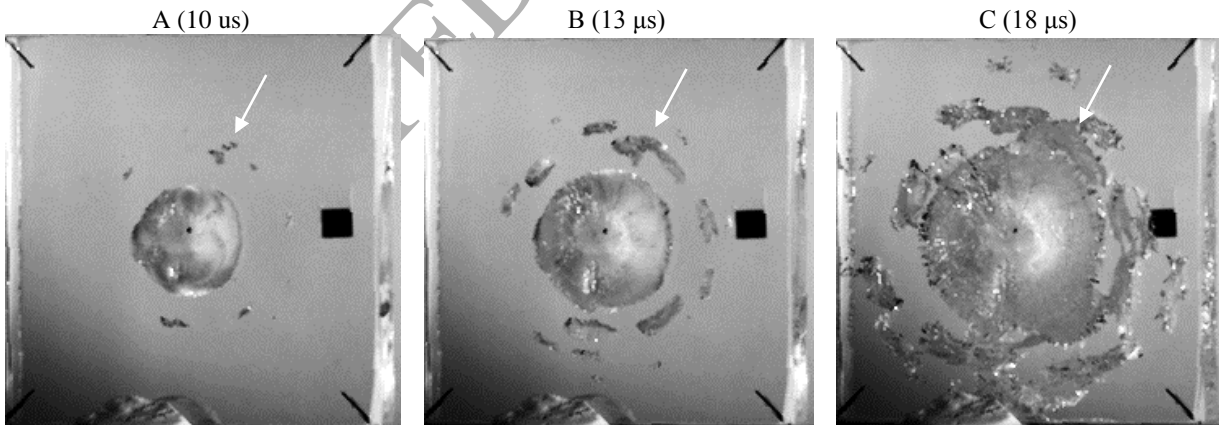


Figure 9: Progression of damage for a 500 m/s impact (arrow indicates growth of discrete fracture ahead of main front).

At velocities where the projectile perforated the target (e.g. 800 m/s), bulk comminution was the dominant mode of failure (Figure 10).

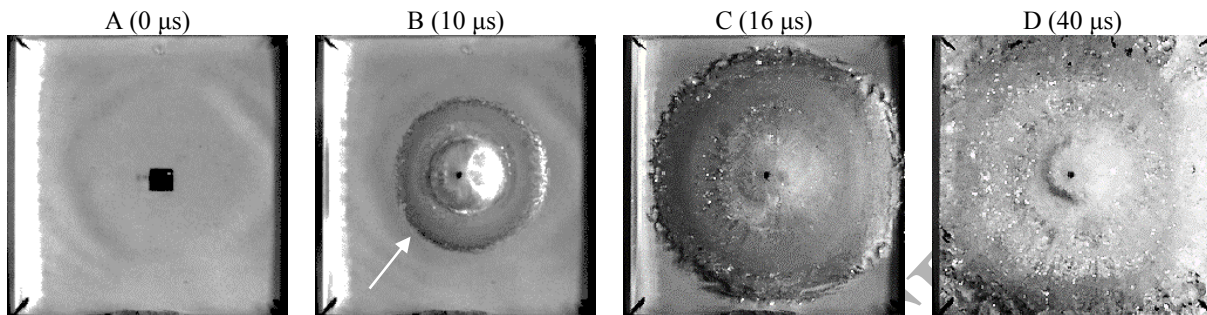


Figure 10: Progression of damage for an 800 m/s impact (arrow indicates damage front).

### 3.3 Damage Front Position with Time

The damage front position was tracked at all impact velocities. The damage front position from the three repeats were averaged to determine trends in the damage front progression (Figure 11). As the impact velocity increased, the extent of the damage also increased. The full experimental damage front displacements and velocities for all experiments are included in Appendix C.

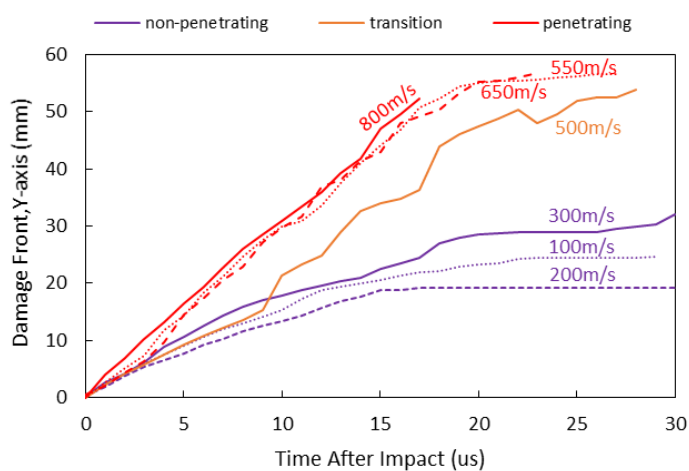


Figure 11: Averaged damage front position versus time for all impact velocities.

## 4. Discussion

### 4.1 Test Methodology

The kinematics camera (Camera A) had a sufficient frame rate to measure the initial and final velocity of the projectile; however, at 800 m/s, material ejecta obscured the projectile in two of three tests and the residual velocity could not be measured. Due to the lower frame rate of this camera, through thickness damage propagation could not be measured accurately. Given that the fracture cone forms over approximately  $25 \mu\text{s}$ , a frame rate of 1 000 000 is recommended, and would also require polishing the tile edge (Figure 3) to potentially capture damage evolution in this plane.

The damage camera (Camera B) had a sufficient frame rate to capture the progression of damage for all impact velocities (Figure 7). However, the resolution was limited to  $420 \times 250$ , which was further reduced to  $240 \times 240$  once cropped to fit the target. This resulted in a spatial resolution of 0.4 mm per pixel, which worked well for position measurements, but not as well for determining crack propagation velocities. A deviation of one pixel would result in a velocity difference of 423 m/s, making velocity measurements of fracture and damage fronts approximate. One possible future modification would be to record a quarter of the target at the same resolution as suggested by Anderson et al. (2014), effectively halving this error.

## 4.2 Damage Mechanisms in Glass Tile

The impact tests results could be divided into three regimes based on the residual velocities of the projectiles: perforating events where the sphere defeated the target, non-perforating events where the projectile did not defeat the target, and a transition region between perforating and non-perforating events (Figure 12).

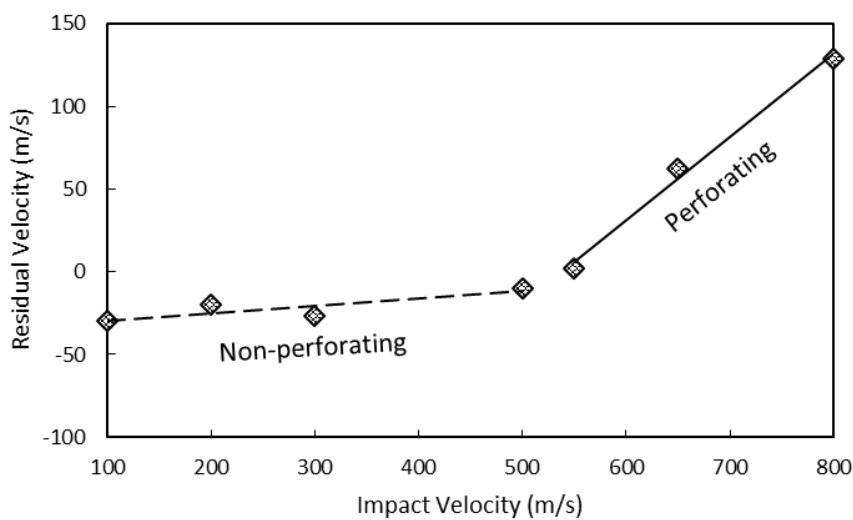


Figure 12: Impact regimes: non-perforating, transition and perforating.

Each of these regimes demonstrated differences in the observable damage features of the targets (Figure 13). In the non-perforating regime (projectile velocities of 100 – 500 m/s), the tile exhibited discrete fracture. At transition velocities (500 – 550 m/s), the dominant mode of failure transitioned from discrete fracture to include some bulk failure that initiated at sites of discrete fracture, including edge cracks. At perforating velocities (550 – 800 m/s), the target failed through bulk comminution, which progressed as a single damage front.

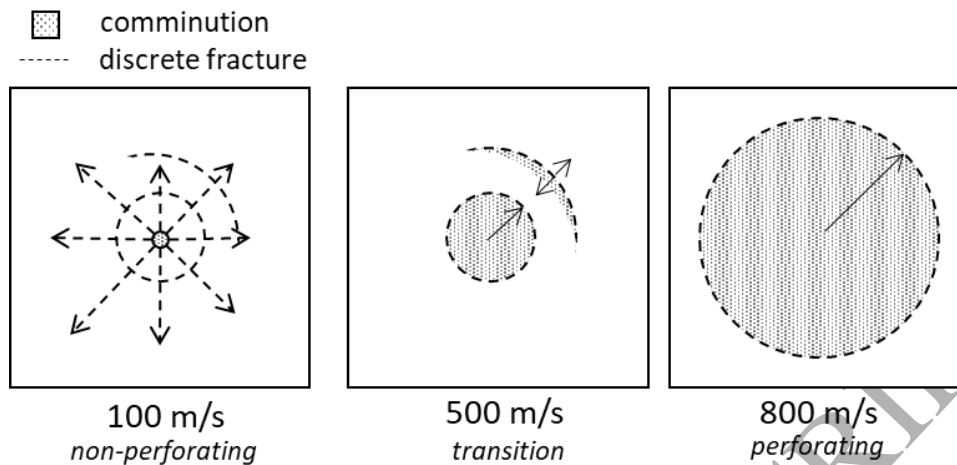


Figure 13: Schematic view of modes of failure.

The transition from perforating to non-perforating was abrupt when comparing damage front displacements over time (Figure 11). There was a clear distinction between non-perforating (purple curves in Figure 11) and perforating (red curves in Figure 11) events. The transition from discrete fracture to bulk comminution was also evident when tracking the damage front velocity over time (Figure 14). In the non-perforating regime, the damage front velocities reached 1500 m/s in agreement with the reported crack velocity (Küppers 1966, Barstow & Edgerton 1939, Nielsen 2009). In the perforating regime, the damage front velocity approached 3270 m/s (Figure 14). This may be indicative of a change in failure mode from discrete fracture to comminution, an observation which is in agreement with measurements made by Grujicic et al. (2009), where they measured comminuted damage front velocities of 3270 m/s in soda-lime glass. Anderson (2014) reported much lower damage front speeds (800 m/s to 1200 m/s); however, those tests were performed on a different type of glass (Borofloat 33) and the targets were bonded to polycarbonate backing, which could explain this difference. In the transition region, the damage front velocity jumped between the crack speed of the material and the

comminution front speed. The damage front velocity measurements in the transition region resulted in greater tracking errors due to the start and stop nature of the damage front (see Appendix C, Figure A8).

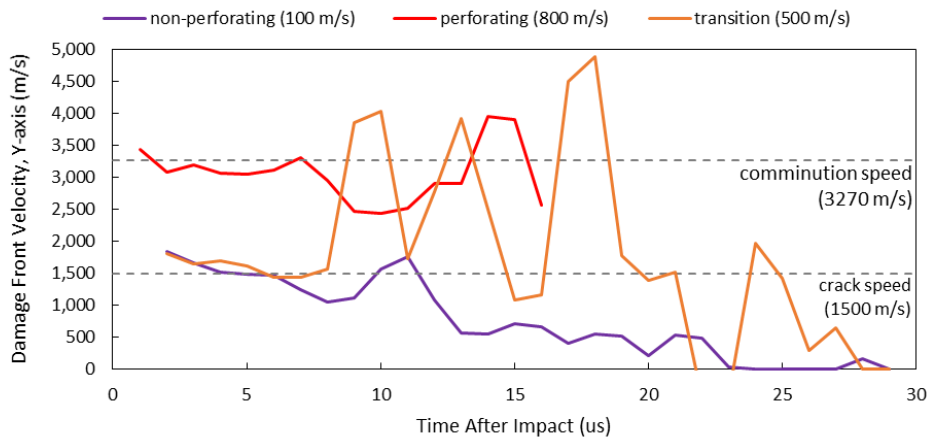


Figure 14: Experimental damage front velocity for non-perforating, transition and perforating impact tests.

## 5. Conclusions

The projectile impact and residual velocities were successfully tracked using high-speed imaging, with some challenges at higher impact velocities due to the ejection of damaged material. A range of damage mechanisms were observed including fracture cones, radial, concentric and edge cracks, as well as material comminution, which was quantified using high speed imaging of the target. Three distinct regimes of impact (non-perforating from 100 – 500 m/s, a transition zone from 500 m/s – 550 m/s and a perforating region from 550 – 800 m/s) were identified, and a transition from discrete failure to comminution was observed with increasing impact velocity. The damage front progression and velocity were measured from the high speed imaging, which indicated a change in damage front velocity from ~1500 m/s (discrete fracture) to ~3270 m/s (comminution), corresponding with the transition from non-perforating to

perforating events. The sphere on glass tile tests were repeatable and consistent for a wide range of impact velocities, providing simple and reproducible boundary conditions that can be used for the comparison of materials and assessment of computational models.

## 6. Acknowledgements

The authors would like to thank the Natural Sciences and Engineering Research Council of Canada, Defence Research and Development Canada - Valcartier Research Centre, Prelco Inc., General Dynamics Land Systems-Canada and the National Research Council Canada for financial and technical support.

ACCEPTED MANUSCRIPT

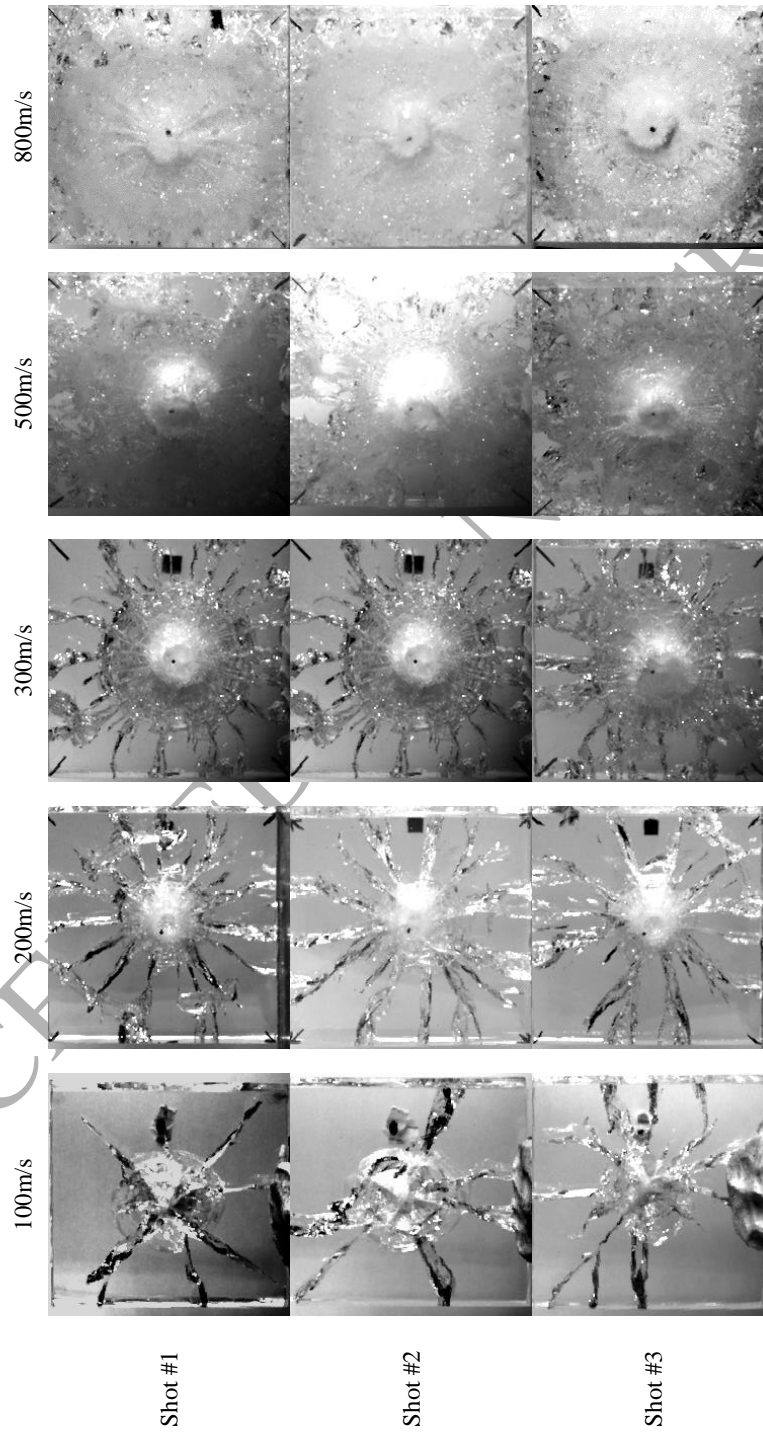
## 7. References

1. Talladay, T. G., & Templeton, D. W. (2014). Glass Armor - An Overview. *International Journal of Applied Glass Science*, 5(4), 331-333. doi:10.1111/ijag.12096
2. Curran, D., Seaman, L., Cooper, T., & Shockey, D. (1994). Micromechanical model for comminution and granular flow of brittle material under high strain rate application to penetration of ceramic targets. *International Journal of Impact Engineering*, 13(1), 53-83. doi:10.1016/0734-743x(93)90108-j
3. Chaudhri, M. M. (2015). Dynamic fracture of inorganic glasses by hard spherical and conical projectiles. *Philosophical Transactions of the Royal Society A: Mathematical, Physical and Engineering Sciences*, 373(2038), 20140135-20140135. doi:10.1098/rsta.2014.0135
4. Meyers, M. A. (1994). *Dynamic behavior of materials*. New York: John Wiley & Sons.
5. Wilkins, M. L. (1978). Mechanics of penetration and perforation. *International Journal of Engineering Science*, 16(11), 793-807. doi:10.1016/0020-7225(78)90066-6
6. Shockey, D. A., Marchand, A., Skaggs, S., Cort, G., Burkett, M., & Parker, R. (1990). Failure phenomenology of confined ceramic targets and impacting rods. *International Journal of Impact Engineering*, 9(3), 263-275. doi:10.1016/0734-743x(90)90002-d
7. Küppers, H. (1967). The initial course of crack velocity in glass plates. *International Journal of Fracture Mechanics*, 3(1). doi:10.1007/bf00188641
8. Barstow, F. E., & Edgerton, H. E. (1939). Glass-Fracture Velocity. *Journal of the American Ceramic Society*, 22(1-12), 302-307. doi:10.1111/j.1151-2916.1939.tb19471.x
9. Nielsen, J. H., Olesen, J. F., & Stang, H. (2008). The Fracture Process of Tempered Soda-Lime-Silica Glass
10. Grujicic, M., Panduragangan, B., Coutris, N., Cheeseman, B. A., Fountzoulas, C., Patel, P., . . . Bishnoi, K. (2009). A simple ballistic material model for soda-lime glass. *International Journal of Impact Engineering*, 36(3), 386-401.
11. Dannemann, K. A., Anderson, C. E., Chocron, S., & Spencer, J. F. (2011). Damage Development in Confined Borosilicate and Soda-Lime Glasses. *Journal of the American Ceramic Society*, 95(2), 721-729. doi:10.1111/j.1551-2916.2011.04969.x
12. Chaudhri, M. M., & Walley, S. M. (1978). Damage to glass surfaces by the impact of small glass and steel spheres. *Journal of Materials Science*, 12(8), 1573-1586. doi:10.1080/01418617808235430
13. Thornton, J. I., & Cashman, P. J. (1986). Glass Fracture Mechanism—A Rethinking. *Journal of Forensic Sciences*, 31(3), 818-824. doi:10.1520/jfs11092j



14. Straßburger, E. (2009). Ballistic testing of transparent armour ceramics. *Journal of the European Ceramic Society*, 29(2), 267-273. doi:10.1016/j.jeurceramsoc.2008.03.049
15. Anderson, C. E., Bigger, R. P., & Weiss, C. E. (2014). Crack and Damage Velocities in Ballistic Experiments. *International Journal of Applied Glass Science*, 5(4), 374-383. doi:10.1111/ijag.12091
16. Hazell, P. J. (2010). Measuring the strength of brittle materials by depth-of-penetration testing. *Advances in Applied Ceramics*, 109(8), 504-510. doi:10.1179/174367610x12804792635387
17. Compton, B. G., Gamble, E. A., & Zok, F. W. (2013). Failure initiation during impact of metal spheres onto ceramic targets. *International Journal of Impact Engineering*, 55, 11-23. doi:10.1016/j.ijimpeng.2012.12.002
18. Strassburger, E., Patel, P., McCauley, J. W., Kovalchick, C., Ramesh, K. T., & Templeton, D. W. (2008). High-Speed Transmission Shadowgraphic and Dynamic Photoelasticity Study of Stress Wave and Impact Damage Propagation in Transparent Materials and Laminates Using the Edge-On Impact (EOI) Method. United States: Army research lab aberdeen proving ground md.
19. Willmott, G. R., & Radford, D. D. (2005). Taylor impact of glass rods. *Journal of Applied Physics*, 97(9), 093522. doi:10.1063/1.1889249
20. Haney, E., & Subhash, G. (2012). Damage Mechanisms Perspective on Superior Ballistic Performance of Spinel over Sapphire. *Experimental Mechanics*, 53(1), 31-46. doi:10.1007/s11340-012-9634-0
21. Zhang, X., Hao, H., & Ma, G. (2015). Dynamic material model of annealed soda-lime glass. *International Journal of Impact Engineering*, 77, 108-119. doi:10.1016/j.ijimpeng.2014.11.016
22. Cook, R. F., & Pharr, G. M. (1990). Direct Observation and Analysis of Indentation Cracking in Glasses and Ceramics. *of the American Ceramic Society*, 73(4), 787-817. doi:10.1111/j.1151-2916.1990.tb05119.x
23. Weinhold, C. (2013). U.S. Patent No. US 8,603,616 B1. Washington, DC: U.S. Patent and Trademark Office.

## Appendix A – Damage Propagation Consistency between Repeats

**Figure A1:** Damage view (opposite to point of impact) of experiments at 50 $\mu$ s after impact

## Appendix B – Damage Progression Analysis of Select Tests

Figure A2: 100 m/s – Shot #4

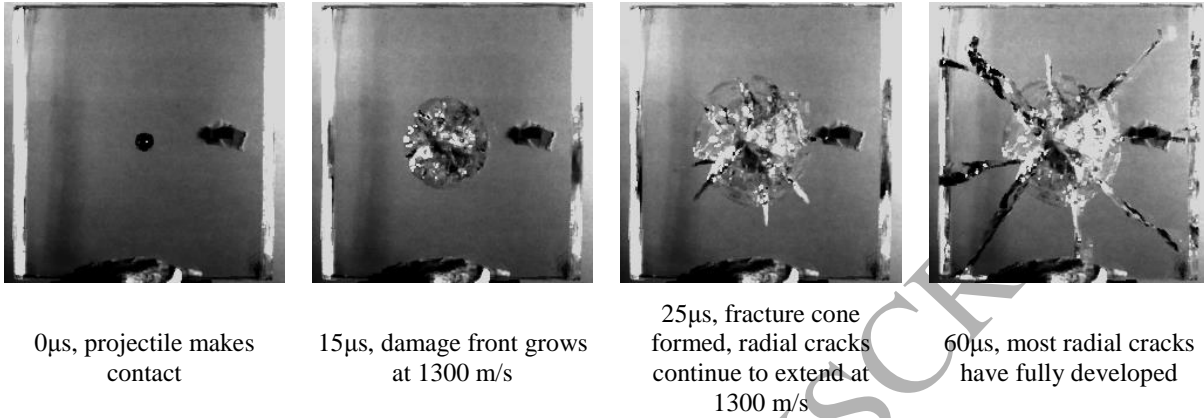


Figure A3: 200 m/s – Shot #44

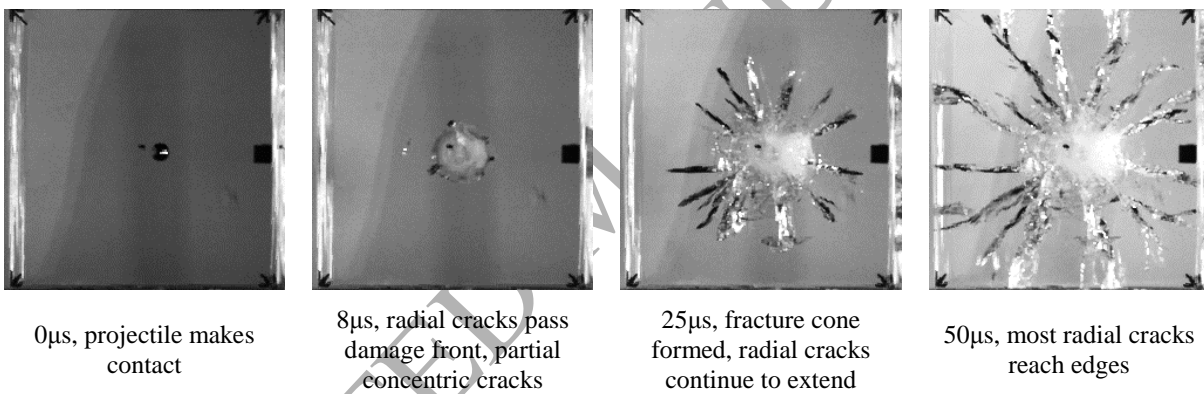
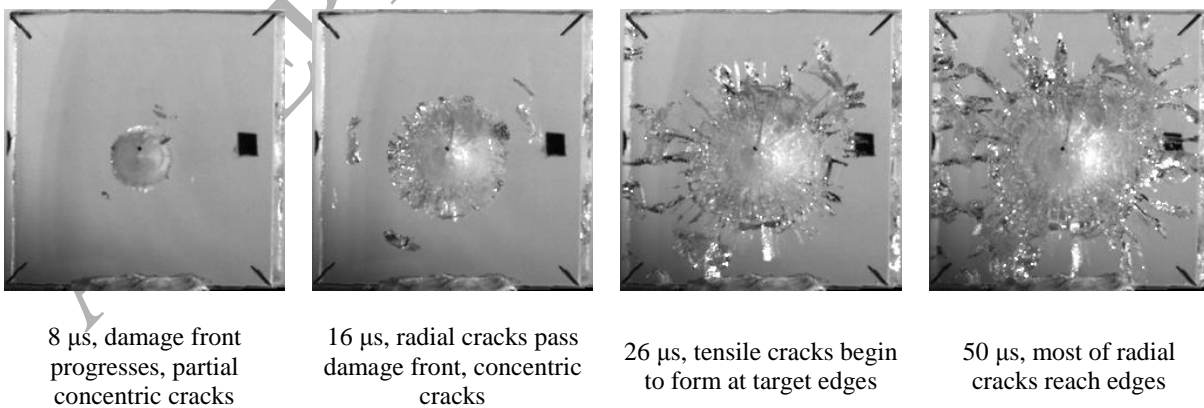
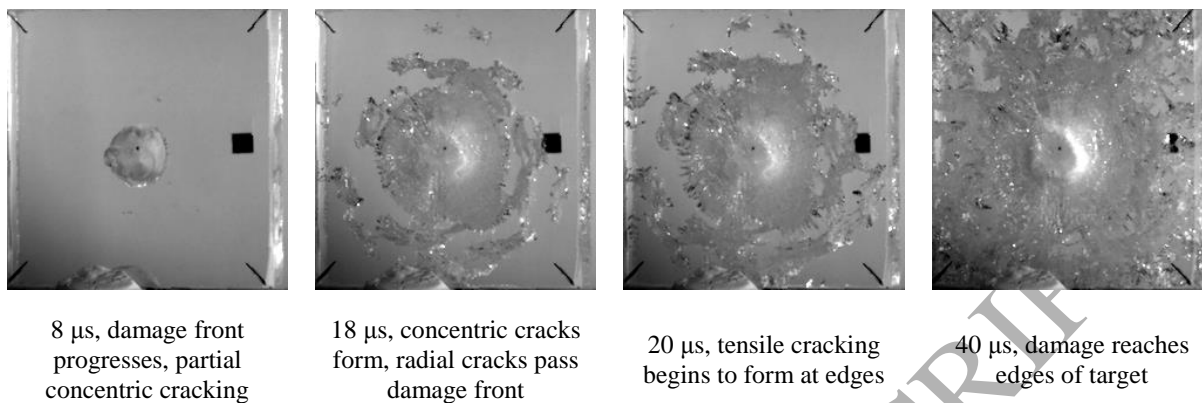
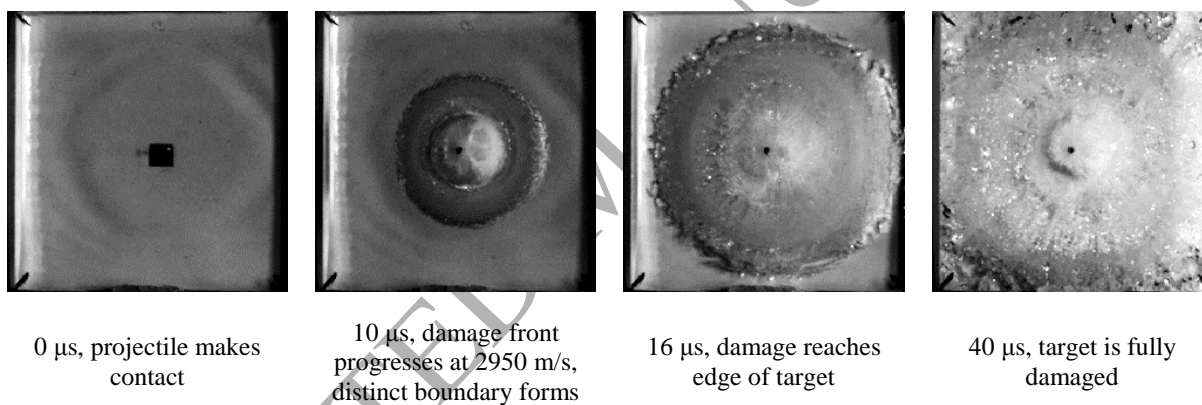
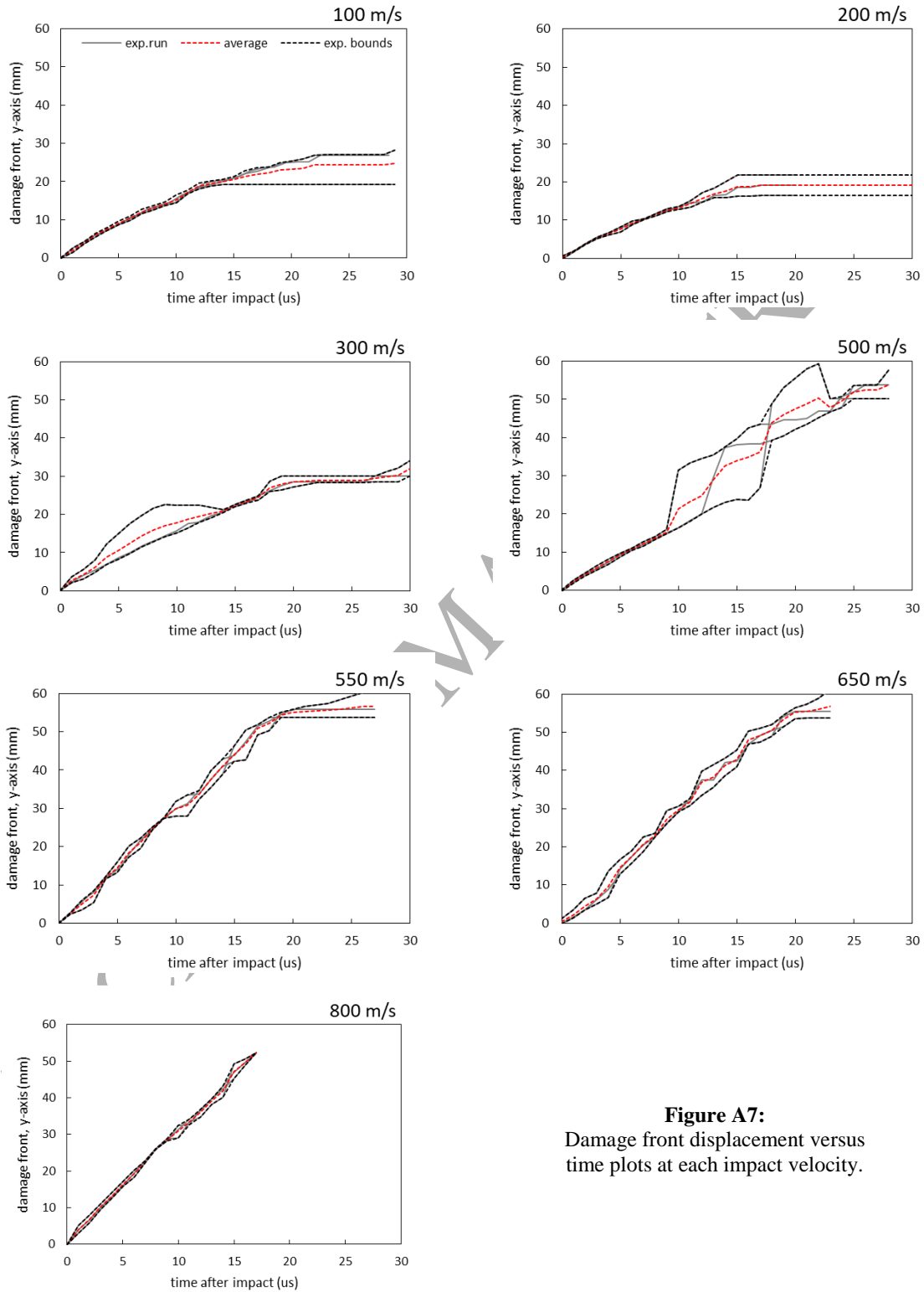


Figure A4: 300 m/s – Shot #23



**Figure A5: 500 m/s – Shot #14****Figure A6: 800 m/s – Shot #74**

## Appendix C – Damage Front Tracking Data



**Figure A7:**  
Damage front displacement versus  
time plots at each impact velocity.

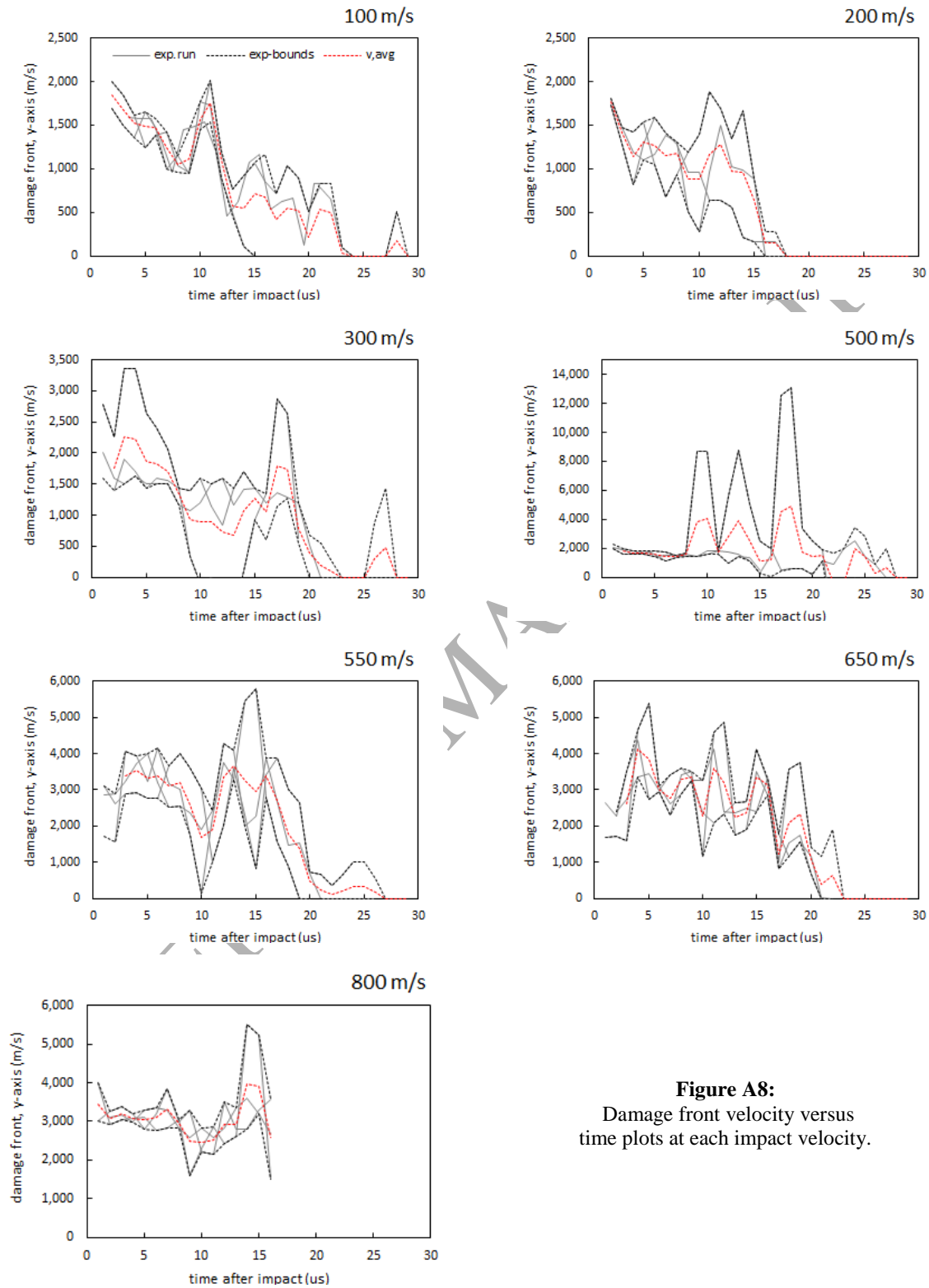


**Figure A8:**  
Damage front velocity versus  
time plots at each impact velocity.